



Development of a cryogenic induction motor for use with a superconducting magnetic bearing

Tomotake Matsumura ^{a,*}, Shaul Hanany ^a, John R. Hull ^b, Bradley Johnson ^c,
Terry Jones ^a, Paul K. Oxley ^a

^a *School of Physics and Astronomy, University of Minnesota, Twin Cities, MN 55455, USA*

^b *Energy Technology Division, Argonne National Laboratory, Argonne, IL 60439, USA*

^c *Cardiff University, 5 The Parade, Queens Buildings Cardiff, CF24 3YB, UK*

Received 23 November 2004; accepted 16 February 2005

Available online 14 July 2005

Abstract

We have constructed a cryogenic induction motor to turn the rotor of a superconducting magnetic bearing (SMB). Both the motor and the SMB are operated at liquid He temperatures. We give a model for the motor and present measurements of its operation. The rotation speed is very stable. Over 8 h it shows an RMS variation of only 0.005 Hz from a mean of 2 Hz. The speed variation within one period of rotation is $3\% \pm 1\%$ implying that the angular position of the rotor can be determined to an accuracy of 1° for all angles of rotation even if angular position is encoded only once every period. Friction and heat dissipation in this motor is dominated by eddy currents. We discuss the application of the motor to astrophysical polarimetry.

© 2005 Elsevier B.V. All rights reserved.

PACS: 85.70.Rp; 95.75.Hi

Keywords: Astrophysical polarimeter; Induction motor; Superconducting magnetic bearings

1. Introduction

Superconducting magnetic bearings (SMBs) have been suggested for use in many applications of rotating systems that require low energy loss [1]. One of the proposed uses is in astrophysical polarimetry. A polarimeter modulates a polarized signal at known frequency by rotating a half-wave

* Corresponding author. Postal address: 116 Church Street SE, Minneapolis, MN 55455, USA. Tel.: +1 612 626 9149; fax: +1 612 626 1080.

E-mail address: tmatsumu@physics.umn.edu (T. Matsumura).

plate (HWP) [2]. The HWP is mounted on a permanent ring magnet that is levitated above a high-temperature superconductor (HTS) to eliminate any stick-slip friction between the rotor and the stator, a source of microphonic noise induced in detectors [2]. In this application the polarimeter operates at liquid helium temperature and the HWP rotates with a constant rotation frequency of about 10 Hz.

Because the polarimeter operates at liquid helium temperature with observation times between hours and years, the rotor has to be driven by a motor which keeps the HWP at a stable rotation speed with low heat dissipation and low noise. We have constructed an induction motor to drive the rotor of the SMB. In this paper we report on the design of the motor and on measurements that characterize its operation.

2. Experimental setup

A sketch of the motor and the experimental setup used to test it is shown in Fig. 1. The motor and the SMB are mounted on the cold plate of a liquid helium cryostat. The rotor of the SMB is a sintered NdFeB permanent magnet ring and the stator is made of an array of 12 melt-textured bulk YBCO tiles. The levitation distance between the magnet and the HTS is 5.5 mm. More details about the SMB are given by Hanany et al. [2].

The motor consists of three stator coils and a copper disk that is mounted to the rotor of the SMB. Each coil is made of a C-shaped molybdenum permalloy powder core that is wound with 1500 turns of copper clad NbTi superconducting wire with diameter of 0.13 mm. The coils are driven with 120° phase-shifted AC current that is supplied by a commercially available linear amplifier [3] placed outside of the cryostat. The gaps of C-shaped coils are located at a radius of 58 mm with respect to the center of the rotor and are tightly packed in azimuth, having in a circumferential separation of about 20 mm as shown in Fig. 1. We found that this configuration maximizes the torque to the rotor; therefore, only three coils provide sufficient torque to overcome friction.

We measure the rotation frequency using an optical encoder. The copper disk has 60 slots along its circumference and serves as an optical chopper for a cryogenic LED and a photodiode that are positioned above and below the disk at the radial location of the slots. More details about this encoder are given by Matsumura et al. [4]. The encoder output is sampled densely in time and analysis of this data gives both position and rotation speed of the rotor as a function of time.

A thin film resistance temperature sensor is mounted in proximity to one of the coils to measure its temperature.

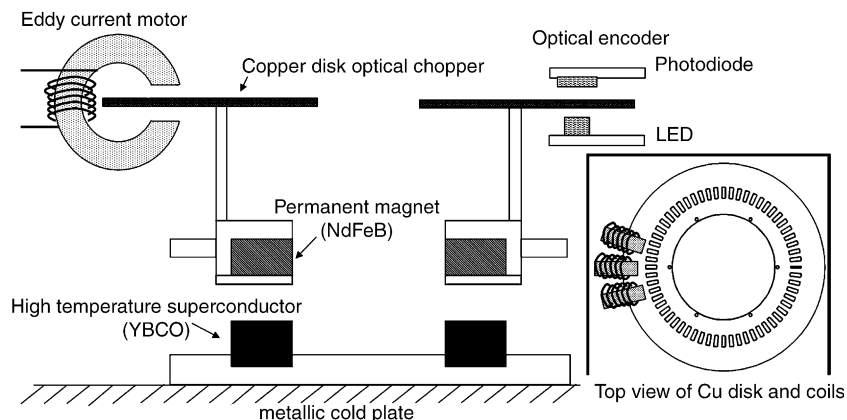


Fig. 1. Cross-sectional view of the motor and hardware used to characterize it. The bottom right inset shows a top view of the motor. The slots in the disk are part of an optical encoder and are not necessary for the motor.

3. Motor model

Richards and Tinkham [5] analyzed the torque due to eddy currents that is applied to an infinitely large conductive plane when a sinusoidal magnetic field wave with a group velocity v_0 travels above it. We adapt their formalism to describe our motor. The equation of motion of the rotor can be written as

$$\frac{\tau}{2\pi} = I_m \dot{f} = A(f_0 - f) - Bf - \frac{C}{2\pi}, \quad (1)$$

where τ is the torque on the rotor, I_m is its moment of inertia, and $f_0 = v_0/2\pi r$, where r is the radial location on the rotor where the motor applies torque. The first term on the right hand side is called the torque due to ‘slip’, that is the difference between the frequency of the traveling wave f_0 and the instantaneous rotation frequency f . There is no torque when the two friction terms on the right hand side balance the driving term coming from slip. The coefficient A can be expressed as

$$A = \bar{A}(\sigma, d)I_c^2 \quad (2)$$

where I_c is the RMS of the current applied to the coils, σ is the electrical conductivity of the conductive plane, and d is its skin depth. The friction terms describe torques that originate from the SMB system and arise from eddy current losses, which are proportional to Bf and hysteresis losses, which are quantified by C . When using this model a correspondence needs to be made between the frequency of the alternating current in the coils of the motor and the frequency of the traveling wave of the magnetic field. For our physical geometry and assuming coils that are equally spaced circumferentially around *the entire* disk this correspondence gives that when the frequency of the alternating current is F the equivalent traveling wave frequency is $f_0 = 0.16F$. Because there are only three coils around a small part of the circumference of the disk we expect this correspondence to be only approximate.

A solution of Eq. (1) gives

$$f(t) = (f_i - f_f)e^{-\alpha t} + f_f, \quad (3)$$

where f_i is the initial frequency, and f_f is the final frequency of rotation,

$$\alpha = \frac{A+B}{I_m}, \quad f_f = \frac{f_0 A - \frac{C}{2\pi}}{A+B} = \frac{f_0 \bar{A} I_c^2 - \frac{C}{2\pi}}{\bar{A} I_c^2 + B}. \quad (4)$$

According to Eqs. (3) and (4) a steady state frequency of rotation f_f is attained exponentially. The exponential time constant is determined by the RMS of the current, by the skin depth, by the electrical conductivity, and by friction. For sufficiently large currents in the coils Eq. (4) gives $f_f = f_0$, which for our geometry is $f_f = 0.16F$.

4. Measurements and results

4.1. Validity of motor model

We measured the temporal evolution of the frequency of rotation by applying periodic changes in the RMS of the current supplied to the coils and then letting the rotor stabilize to a new final rotation speed. The current was changed in steps between 15 mA and 77 mA RMS and the experiment was repeated for alternating current frequencies of $F = 12.5, 25,$ and 50 Hz. Data from one such experiment is shown in Fig. 2. Following Eq. (3) we fit the data with exponentials and extracted α from the exponent of the fit. The agreement between the fit and the data shown in Fig. 2 is representative of the quality of the fit in all cases.

4.2. Source of friction

To measure which of hysteresis or eddy currents is the major source of friction in our motor we let the rotor spin-down freely with the coils not energized. In Fig. 3 we plot the one sample of the data of deceleration as a function of rotation frequency f .

According to Eq. (1) we expect

$$-\frac{df}{dt} = a_0 + a_1 f. \quad (5)$$

A fit to this data gives the fit parameters a_0 and a_1 as $7.3 \times 10^{-4} \text{ s}^{-2}$ and $3.9 \times 10^{-3} \text{ s}^{-1}$, respectively.

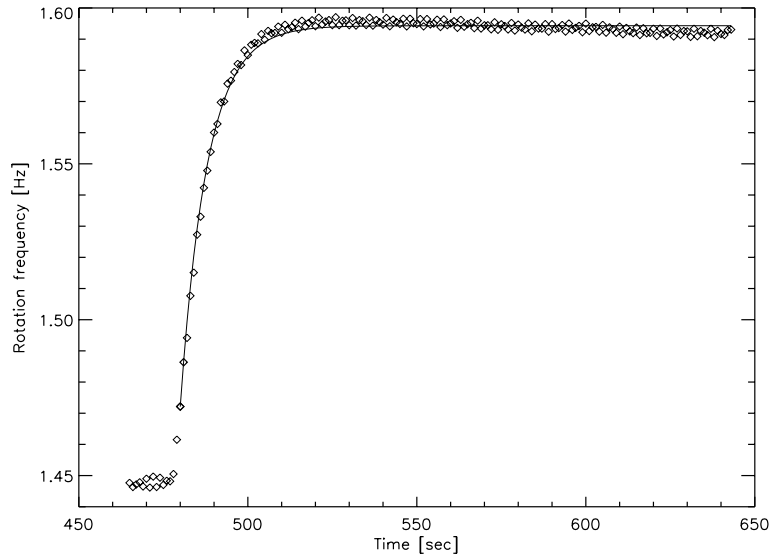


Fig. 2. The rotation frequency as a function of time. The RMS current changed from 32 mA to 53 mA at $t = 470$ s. The rotation frequency increased from its initial state to the final state exponentially. The solid line is a fit to the data after $t = 470$ s using Eq. (3).

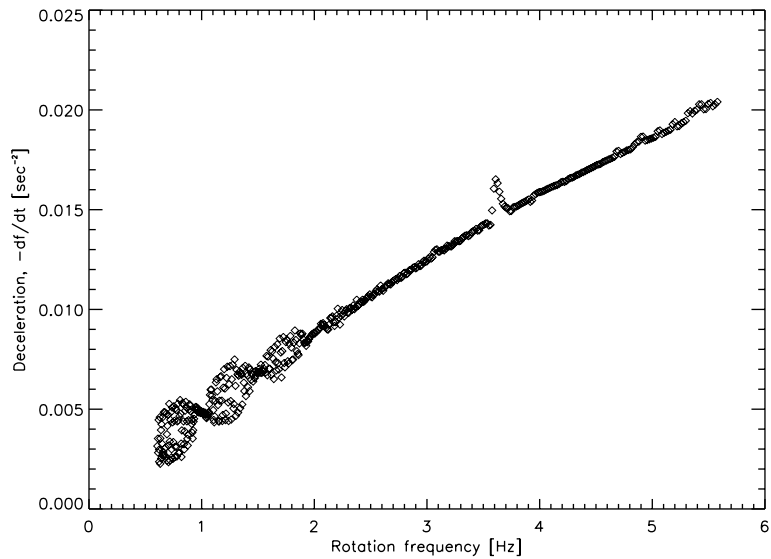


Fig. 3. The deceleration as a function of rotation frequency during a free spin-down of the rotor.

4.3. Long term stability of rotation

It is important to characterize the stability of the rotation over an extended period of time. The top panel of Fig. 4 shows the rotation frequency with a fixed frequency F of 25 Hz and an RMS current

of 39 mA. The rotation frequency stays approximately constant for over 8 h of measurement. The bottom panel shows the power spectral density of the rotation frequency after subtraction of a mean over 8 h. The RMS variation is 5.4×10^{-3} Hz for time scales between 2 s and 8 h.

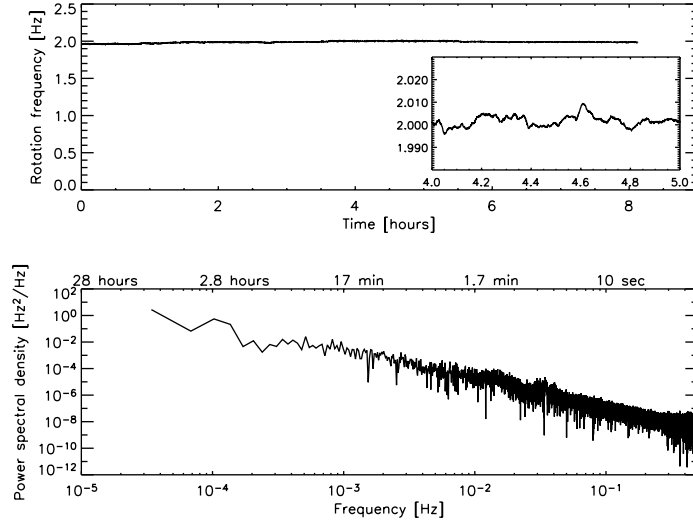


Fig. 4. Top panel: stability of rotation frequency as a function of time. The inset shows a zoom on the data between 4 and 5 h with an expanded scale for the vertical axis. Bottom panel: power spectral density of the data in the top panel after subtraction of a mean.

4.4. Variation of rotation frequency within a single period

Using our data we extracted the variation of the rotation frequency within a single period of rotation. A description of the technique is given by Matsumura et al. [4]. The fractional speed variation, δ , is defined as

$$\delta = \frac{\Delta f_{pp}}{\bar{f}}, \quad (6)$$

where Δf_{pp} is the peak to peak rotation frequency variation from its mean \bar{f} within one cycle of rotation. Over the 8 h of data shown in Fig. 4 we find $\bar{\delta} = 3.4 \pm 1\%$.

4.5. Heat dissipation in the coils

In Fig. 5 we plot the temperature of coil as a function of the frequency F . We have also found that the temperature of the coils remains below 5 K when the RMS current to the coil is below 60 mA and the frequency is below 25 Hz.

5. Discussion and conclusions

There appears to be agreement between our model for the motor and the data. The temporal

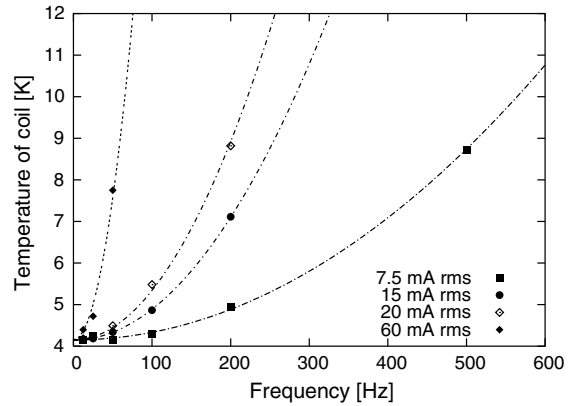


Fig. 5. The temperature of the coil as a function of frequency of the applied current for RMS currents of 7.5 mA, 15 mA, 20 mA, and 60 mA.

evolution of the rotation speed follows an exponential, as expected from Eq. (3). Fig. 6 shows the exponent α as a function of the RMS of the AC current for the three different frequencies f_0 . The data shows a quadratic dependence on the current in agreement with Eqs. (2) and (4). When we apply sufficiently large currents the frequency f_r does approach the expected value f_0 as predicted by Eq. (4).

The interpretation of the data in terms of the model is subject to some uncertainty because of

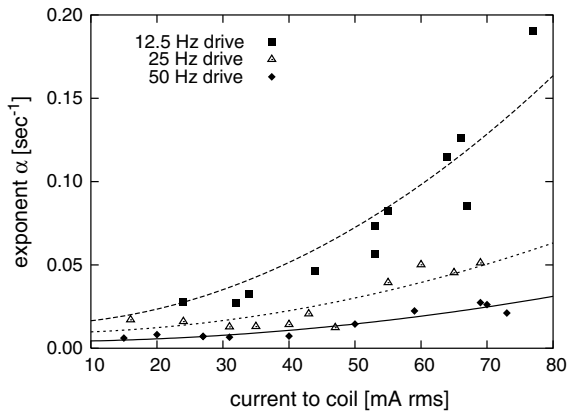


Fig. 6. The exponent α as a function of the RMS current for frequencies of 12.5, 25, and 50 Hz. The continuous lines are quadratic fits to the data of each of the frequencies.

uncertainty in the temperature of the rotor. For a fixed frequency f_0 the torque of the motor depends on the electrical conductivity of the disk, which is a function of its temperature. The change in the RMS of the driving current results in a change in the RMS of eddy currents in the disk and therefore a change in heat dissipation. Because the disk is levitated and has no conductive or convective thermal path to the environment its heating or cooling time scale is long compared to the duration of accelerations or decelerations, and therefore the temperature of the disk may not be stabilized during our measurements.

Our experiments show that the coefficient of friction in our bearing system is dominated by losses due to eddy currents and not due to hysteresis. This indicates that the presence of the motor increases the friction due to eddy currents because the same experimental setup without the motor gave friction which was dominated by losses from hysteresis [2].

It is interesting to measure the fractional speed variation $\bar{\delta}$ because it informs the decision about the angular encoding of the SMB [4]. Previous measurements by our group [4] gave an upper limit of 1% for $\bar{\delta}$ at rotation frequency above 1 Hz when the rotor was not driven. The 1% limit was due to noise that originated from the translational vibration of the rotor. We find an increase of $\bar{\delta}$ to a level

of 3.4% in the presence of drive torque due to the motor. If we assume that the entire contribution to $\bar{\delta}$ comes purely from an actual change in rotation frequency, and is not induced by e.g. a translational motion of the rotor, we calculate that an angular encoding of the position of the rotor only once during a full period would give an upper limit on the uncertainty in the determination of angular position of only 1° . Such accuracy may be adequate for many polarimeters.

The temperature rise of the coil depends on both the RMS and frequency of the applied AC current. Possible heat inputs are Joule heating in the coils, hysteresis loss in the core and in the coils, and eddy currents in the core, in the copper cladding of the coils, and in metallic elements near the coils. The data of Fig. 5 shows a quadratic nature of the increase in temperature with respect to frequency F , which suggests that the source of heat are eddy currents. This conclusion relies on the assumption that the thermal conductance between the source of heat and the thermometer stays approximately constant as a function of temperature.

We have identified a range of operation parameters for the motor where the temperature of the coil remains stable and far below the critical temperature of the superconducting NbTi wire of the coils.

Acknowledgement

The author would like to thank Dr. Ki Ma for the useful discussion.

References

- [1] J.R. Hull, Supercond. Sci. Technol. 13 (2000) R1.
- [2] S. Hanany, T. Matsumura, B. Johnson, T. Jones, J.R. Hull, K.B. Ma, IEEE Trans. Appl. Superconduct. 13 (June) (2003) 2128.
- [3] Trust Automation Inc., TA 310 linear amplifier.
- [4] T. Matsumura, S. Hanany, J.R. Hull, B. Johnson, T. Jones, presented in Applied Superconductivity Conference 2004, Jacksonville Florida, IEEE Trans. Appl. Superconduct., in press.
- [5] P.L. Richards, M. Tinkham, J. Appl. Phys. 43 (1972) 2680.